ACS APPLIED MATERIALS & INTERFACES

Research Article

www.acsami.org

Polyaniline Stabilized Magnetite Nanoparticle Reinforced Epoxy Nanocomposites

Hongbo Gu,[†,‡] Sruthi Tadakamalla,[†,§] Yudong Huang,*[,‡] Henry A. Colorado,[⊥,▽] Zhiping Luo,[#] Neel Haldolaarachchige,[∥] David P. Young,[∥] Suying Wei,*[,§] and Zhanhu Guo*[,†]

[†]Integrated Composites Lab (ICL), Dan F. Smith Department of Chemical Engineering, and [§]Department of Chemistry and Biochemistry, Lamar University, Beaumont, Texas 77710, United States

[‡]School of Chemical Engineering and Technology, Harbin Institute of Technology, Harbin, Heilongjiang 150001, China

[⊥]Materials Science and Engineering, University of California, Los Angeles, California 90095, United States

[#]Microscopy and Imaging Center, and Materials Science and Engineering Program, Texas A&M University, College Station, Texas 77843, United States

[∥]Department of Physics and Astronomy, Louisiana State University, Baton Rouge, Louisiana 70803, United States

Supporting Information

ABSTRACT: Magnetic epoxy polymer nanocomposites (PNCs) reinforced with magnetite (Fe_3O_4) nanoparticles (NPs) have been prepared at different particle loading levels. The particle surface functionality tuned by conductive polyaniline (PANI) is achieved via a surface initiated polymerization (SIP) approach. The effects of nanoparticle loading, surface functionality, and temperature on both the viscosity and storage/loss modulus of liquid epoxy resin suspensions and the physicochemical properties of the cured solid PNCs are systematically investigated. The glass transition temperature (T_g) of the cured epoxy filled with the functionalized NPs has shifted to the higher temperature in the dynamic mechanical analysis (DMA) compared with that of the cured pure epoxy. Enhanced mechanical properties of the cured epoxy PNCs filled with the functionalized NPs are observed in the tensile test compared with that of the cured pure epoxy and cured epoxy PNCs filled with as-received NPs. The uniform NP distribution in the cured epoxy PNCs filled with functionalized NPs is observed by scanning electron microscope (SEM). These magnetic epoxy PNCs show the good magnetic properties and can be attached by a permanent magnet. Enhanced interfacial interaction between NPs and epoxy is revealed in the fracture surface analysis. The PNCs formation mechanism is also interpreted from the comprehensive analysis based on the TGA, DSC, and FTIR in this work.

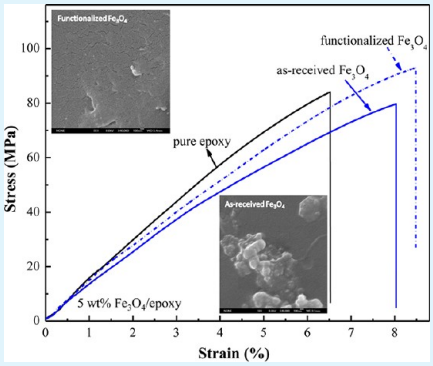

KEYWORDS: *epoxy resin nanocomposites, particle−polymer interaction, viscoelastic property, tensile properties, magnetic properties*

INTRODUCTION

Epoxy resins are very conventional and important engineered thermosetting polymers because of their high tensile strength, Young's modulus, and good thermal and electrical insulating properties[1,2] and potential wide applications including adhesives,[3] electronics (excellent electrical insulators),[4] marine and aerospace.[5,6] The mechanical properties of epoxy can be improved by the introduction of strong inorganic fillers by forming polymer nanocomposites (PNCs), which can also have unique properties such as optical,[7] anticorrosive,[8] electrical,[9,10] and magnetic properties.[11] However, there are still two main challenges to obtain high-performance PNCs. One is the nanofiller dispersion quality in the polymer matrix and the other is the interfacial interaction between the fillers and the hosting polymer matrix. These challenges are much more obvious for the fillers at nanoscale size level because of their easy agglomeration and large specific surface area.[12−14] The poor interfacial compatibility/bonding between the polymer matrix and nanofillers will serve as the crack initiating points and even worsen the mechanical properties. Nanofiller surface treatment is a common way to improve dispersion problem and enhance interfacial polymer−filler interaction[9] through using proper coupling agents,[13,15] surfactants,[16] and polymers.[17] Although many surface treatment methods have been experimentally proved to be efficient,[18] polyaniline (PANI) with the presence of unique amine and imine groups in its backbone[19] to improve the nanofiller dispersion and interfacial interaction by serving as coupling agent has been rarely reported.

Because of the low toxicity, relatively high saturation magnetization (M_s, 92−100 emu g^{-1} at room temperature),[20] and biocompatibility, magnetite (Fe_3O_4) has shown admirable applications including magnetic data storage,[21] catalysts,[22] drug delivery targeting,[23] electrochemical activity,[24] and adsorbents for removing hazardous heavy metals.[25] The introduction of

Received: August 1, 2012
Accepted: September 17, 2012
Published: September 17, 2012

Fe_3O_4 into polymer matrix can provide matrix magnetic properties and enhance mechanical properties, which could broaden their engineered applications, such as microwave adsorption,[26−28] magnetic resonance imaging (MRI),[29] biomedical sensors,[30,31] catalysts,[32] electromagnetic interference shielding, flexible electronics, magneto-optical storage,[33] heavy metal removal,[34,35] magnetochromatic materi,al[36] and magnetic shape memory.[37] However, with scarcity of surface functional groups on the Fe_3O_4 NPs, the subsequent poor epoxy-nanoparticle interaction will weaken the mechanical properties. And the easily agglomerated Fe_3O_4 NPs arising from the interparticle magnetic dipole−dipole interactions[38] and high specific surface area make the dispersion of NPs more difficult.

Rheological property is one of the important properties for studying the processing and applications of epoxy and its PNCs.[39] It is also important to understand the fluid dynamics and statics of the confined polymers and to disclose the nature and microstructures of the epoxy PNCs.[40] Dynamic rheology can be used to estimate the dispersion of the nanofillers in the polymer matrix.[41] Many studies have focused on the dynamic rheological properties of the thermoplastic material melts[42−44] and much less work has been reported on the thermosetting materials.[45]

In the present work, the magnetic epoxy nanocomposites reinforced with Fe_3O_4 NPs were successfully prepared. The surface functionalization of Fe_3O_4 NPs with polyaniline (PANI) was achieved using the surface initiated polymerization (SIP) method. The effects of nanoparticle loading, surface functionality, and temperature on the viscosity and storage/loss modulus of the epoxy resin suspensions were studied systematically. The mechanical properties including dynamic mechanical analysis (DMA) and tensile tests, and magnetic properties of these cured PNCs were studied as well. The fracture surface of the cured epoxy PNCs was observed by scanning electron microscope (SEM). The thermo-stability of the epoxy PNCs was studied by thermogravimetric analysis (TGA). The PNCs filled with as-received Fe_3O_4 NPs were also prepared for comparison. The PNCs formation mechanism was also elaborated based on a comprehensive analysis of DSC, TGA, and FT-IR results.

EXPERIMENTAL METHODS AND CHARACTERIZATION

Materials. The Epon 862 (bisphenol F epoxy) and the curing agent EpiCure W were provided by Miller-Stephenson Chemical Company, Inc. (The molecular structures of these chemicals are shown in Scheme S1, in the Supporting information). Aniline (C_6H_7N), ammonium persulfate (APS, $(NH_4)_2S_2O_8$) and p-toluene sulfonic acid (PTSA, $C_7H_8O_3S$) were purchased from Sigma Aldrich. Methanol was purchased from Fisher Scientific. Fe_3O_4 NPs with an average size of 12 nm were obtained from Nanjing Emperor Nano Material Co., Ltd. All the chemicals were used as-received without any further treatment.

Surface Functionalization of Fe_3O_4 NPs. Fe_3O_4 NPs were functionalized with PANI via a facile SIP method.[46−48] Briefly, Fe_3O_4 NPs (6.696 g), PTSA (15 mmol) and APS (9 mmol) were added into 100 mL deionized water in an ice-water bath for one-hour mechanical stirring (SCILOGEX OS20-Pro LCD Digital Overhead Stirrer, 300 rpm) combined with sonication (Branson 8510). Then the aniline solution (18 mmol in 25 mL deionized water) was mixed with the above Fe_3O_4 nanoparticle suspension and then mechanically stirred under ultrasonication for additional one and half hours in an ice-water bath for further polymerization. The product was vacuum filtered and washed with deionized water until pH value was about 7. The precipitant was further washed with methanol to remove any possible oligomers. The final powders were dried at 50 °C overnight. Pure PANI was also synthesized following the aforementioned procedures without adding NPs for comparison.

Preparation of Fe_3O_4/Epoxy Resin PNCs Suspension. Epon resin suspension containing 2, 5, 10, and 15 wt % of the as-received (untreated) Fe_3O_4 (u-Fe_3O_4) NPs and functionalized Fe_3O_4 (f-Fe_3O_4) NPs were prepared. Both u-Fe_3O_4 and f-Fe_3O_4 NPs were immersed with Epon resin overnight without any disturbance so that the resin can wet the NPs and the solution was then mechanically stirred for one hour (600 rpm, Heidolph, RZR 2041). All the procedures were carried out at room temperature.

Curing of the Fe_3O_4/Epoxy Resin PNCs. The curing agent EpiCure W was added into epon monomers or the above prepared Fe_3O_4 NPs suspended epon resin solutions with a monomer/curing agent weight ratio of 100/26.5 following the recommendation from the Miller-Stephenson Chemical Company for one hour mechanical stirring (200 rpm). Then the solution was mechanically stirred at 70 °C for 2−3 h in a water bath at the same speed (200 rpm), which is essential to remove the bubbles and to prevent the sedimentation of the Fe_3O_4 NPs during the curing process. Finally, the solutions were poured into silicon molds, cured at 120 °C for 5 h, and then cooled to room temperature naturally.

Morphology. The morphologies of the as-received and functionalized Fe_3O_4 NPs and fracture surfaces of the epoxy PNCs were observed on a JSM-6700F system with a JEOL field emission scanning electron microscope (SEM). The SEM specimens were prepared by sputter coating a thin gold layer approximately 3 nm thick. The morphologies of the as-received and functionalized Fe_3O_4 NPs were further characterized by a transmission electron microscopy (TEM, FEI Tecnai G2 F20) with a field-emission gun, operated at an accelerating voltage of 200 kV. The TEM samples were prepared by drying a drop of ethanol suspension on carbon-coated copper TEM grids.

FT-IR Characterization. The chemical structure of u-Fe_3O_4 NPs, f-Fe_3O_4 NPs, and pure PANI was analyzed by a Fourier transform infrared spectroscopy (FT-IR, a Bruker Inc. Vector 22 coupled with an ATR accessory) in the range of 500−4000 cm^{-1} with a resolution of 4 cm^{-1}.

Thermal Property. The thermal stability was studied in a thermogravimetric analysis (TGA, TA Instruments, Q-500) with a heating rate of 10 °C min^{-1} under an air flow rate of 60 mL min^{-1} from 25 to 800 °C.

Rheology. The viscosity of the liquid epon suspensions was studied in a Rheometer (TA Instrumental, AR2000ex ETC system). The measurements were performed in a cone−plate geometry with a diameter of 40 mm and a truncation of 64 μm. The steady state flow procedure was used and the measurements were done at 25, 70, and 120 °C, respectively. The shear rate was carried out between 1 to 1000 1/s. The frequency sweeping between 1 and 100 rad/s was carried out at a low strain (1%), which was justified to be within the linear viscoelastic (LVE) range. The LVE range was determined by the strain-storage modulus (G′) curve within the strain range from 0.1 to 100 % at a frequency of 1 rad/s. The specimens placed between the cone and plate were allowed to equilibrate for approximately two minutes prior to each test.

Mechanical Property. Dynamic mechanical analysis (DMA) was performed in the torsion rectangular mode by using an AR 2000ex (TA Instrumental Company) with a strain of 0.05%, a frequency of 1 Hz and a heating rate of 2 °C min^{-1} in the range of 30-250 °C. The sample dimensions are 12 × 3 × 40 mm^3. Tensile tests were carried out following the American Society for Testing and Materials (ASTM, 2002, standard D412-98a) in a unidirectional tensile test machine (ADMET tensile strength testing system 2610). The parameters (displacement and force) were controlled by a digital controller (MTESTQuattro) with MTESTQuattro Materials Testing Software. The samples (dog-bone shaped) were designed according to the ASTM standard requirement and prepared as described for epoxy PNCs in the molds. A crosshead speed of 1 mm/min was used and the strain (mm/mm) was calculated by dividing the jogging displacement by the original gage length.

Magnetic Property. The magnetic properties were investigated in a 9-Tesla Physical Properties Measurement System (PPMS) by Quantum Design at room temperature.

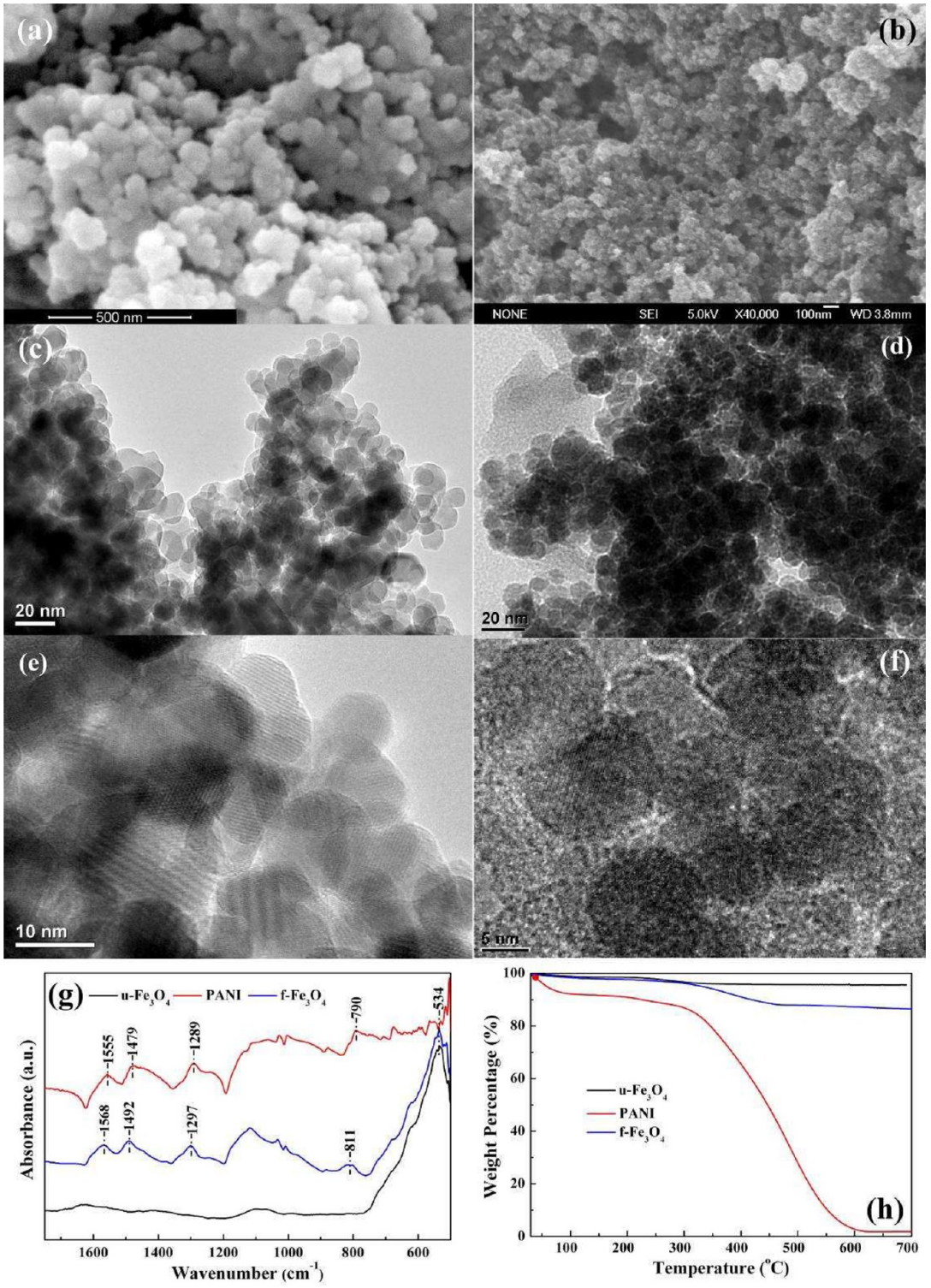

Figure 1. SEM images of (a) u-Fe_3O_4 NPs, (b) f-Fe_3O_4 NPs; TEM images of (c, e) u-Fe_3O_4 NPs, (d, f) f-Fe_3O_4 NPs; (g) FT-IR spectra of pure PANI, u-Fe_3O_4 and f-Fe_3O_4 NPs; and (h) TGA curves of pure PANI, u-Fe_3O_4 and f-Fe_3O_4 NPs.

To investigate the PNCs formation mechanism, we prepared the f-Fe_3O_4 NP and PANI NP samples for the test following the curing procedures without adding the curing agent. First, f-Fe_3O_4 NPs (15 wt % loading) (or PANI) were mechanically stirred (600 rpm) with epoxy resin monomers at room temperature for one hour and then performed at the low speed mechanical stirring (200 rpm) at 70 °C for 2 h. Finally, the suspended solution was cured at 120 °C for 5 h and then cooled to room temperature naturally. The final sticky solution was washed with excessive acetone and vacuum filtered to remove any epoxy monomers. The obtained powders were dried in an oven overnight at 50 °C for FT-IR and TGA tests. The small amount of sticky solution was used to do the TGA and DSC test. DSC measurements were carried in DSC Q2000 (TA Instruments) under a nitrogen flow rate of approximately 20 mL/min at a heating rate of 10 °C/min from 30 to 70 °C and an isothermal process at 70 °C was continued for 2 h. After that, the temperature was continuously increased to 120 °C at a heating rate of 10 °C/min and an isothermal process was conducted at 120 o°C for another 2 h.

dx.doi.org/10.1021/am301529t | ACS Appl. Mater. Interfaces 2012, 4, 5613−5624

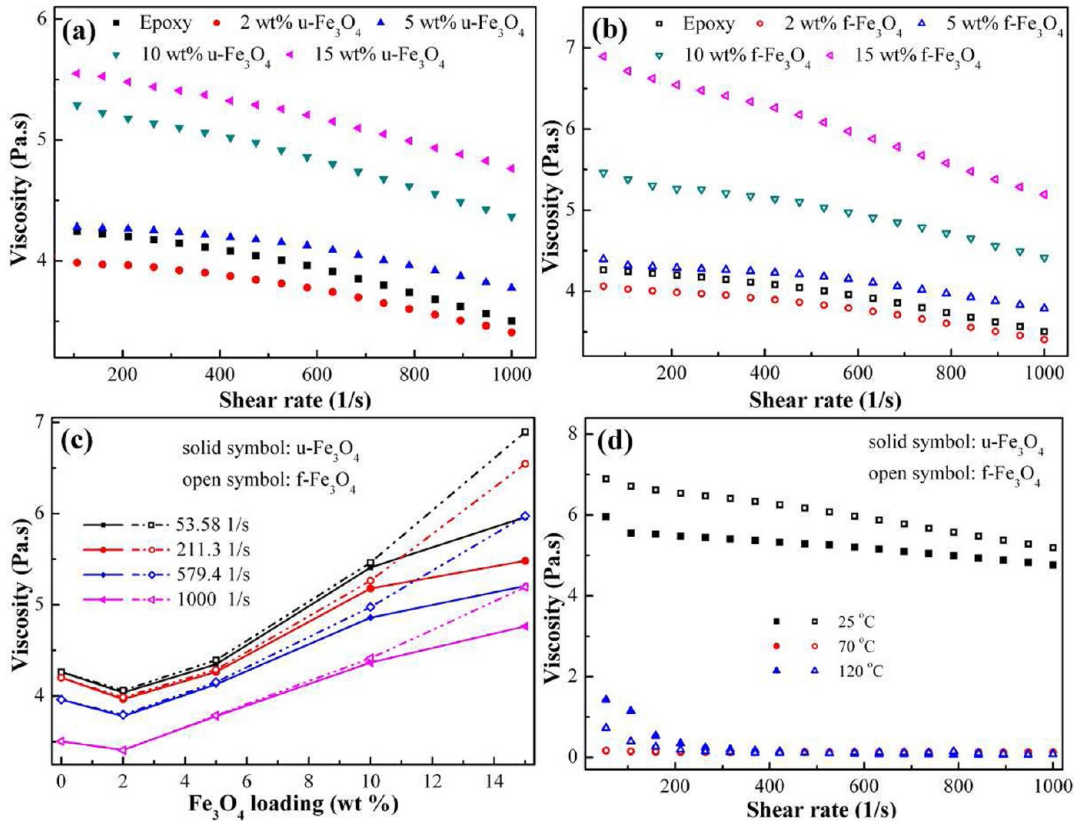

Figure 2. Viscosity vs. shear rate of epoxy resin suspensions filled with different loadings of (a) u-Fe_3O_4 NPs and (b) f-Fe_3O_4 NPs at 25 °C; (c) Effect of surface functionalization on the viscosity of Fe_3O_4/epoxy nanocomposite suspensions with different loadings under different shear rates at 25 °C; (d) Effect of temperature on the viscosity of epoxy resin suspensions with a Fe_3O_4 particle loading of 15 wt %.

RESULTS AND DISCUSSION

Functionalization of Fe_3O_4 NPs. Figure 1 shows the SEM and TEM images of the u-Fe_3O_4 and f-Fe_3O_4 NPs. The u-Fe_3O_4 NPs show spherical shape with smooth surface, Figure 1a, c, e. However, after functionalization with PANI, the surface becomes relatively rougher, Figure 1b, d, f. After functionalization, a thin PANI layer was observed surrounding the NPs, Figure 1d, f, indicating that the polymerization has occurred on the surface of Fe_3O_4 NPs.[47] These results indicate that the surface functionalization has successfully changed the surface morphology of the Fe_3O_4 NPs. The observed lattice fringes before and after the polymerization indicate the highly crystalline structure of the NPs. The observed comparable size indicated that the used acid during polymerization had negligible effect on the NPs and the formed polymer layer protected the nanoparticle core from etching during the further exposure to acid. Meanwhile, the as-received Fe_3O_4 NPs were observed to be dissolved in hydrochloric acid (1.0 M), however, the f-Fe_3O_4 NPs were not dissolved in acid solution, indicating the presence of a PNAI coating layer surrounding NPs against the dissolution.

The surface functional groups have been verified by FT-IR analysis, Figure 1g showing the FT-IR spectra of u-Fe_3O_4 NPs, f-Fe_3O_4 NPs and pure PANI. In the FT-IR spectrum of u-Fe_3O_4 NPs, only one absorption peak at around 534 cm^{-1} appears, which is attributed to the vibration of Fe−O band.[49] Compared with u-Fe_3O_4 NPs, in the FT-IR spectrum of f-Fe_3O_4 NPs, the vibration of Fe−O band is also observed at 534 cm^{-1}. The strong absorption peaks at 1568 and 1492 cm^{-1} correspond to the C=C stretching vibration of the quinoid and benzenoid rings, respectively.[48] The peak at 1297 cm^{-1} is related to the C−N stretching vibration of benzenoid unit.[50] The peak at around 811 cm^{-1} is due to the out-of-plane bending of C−H in the substituted benzenoid ring.[46] These characteristic peaks (1568, 1492, 1297, and 811 cm^{-1}) are also observed in the FT-IR spectrum of PANI, but have a slight shift (about 8−13 cm^{-1}) compared with the f-Fe_3O_4 NPs, indicating that the surface of the u-Fe_3O_4 NPs has been successfully functionalized by PANI.

The TGA curves of u-Fe_3O_4 NPs, f-Fe_3O_4 NPs and pure PANI are shown in Figure 1h. For the u-Fe_3O_4 NPs, the weight almost has no change within the measurement temperature range. For pure PANI, the significant weight loss before 120 °C in the curve is attributed to the loss of moisture. There are two-stage weight losses for pure PANI and f-Fe_3O_4 NPs from 250 to 600 °C, which are due to the elimination of the dopant anions and thermal degradation of PANI chains, respectively.[51,52] The initial nanoparticle loading for f-Fe_3O_4 calculated based on the total mass of aniline and NPs is 80 wt %. However, the obtained nanoparticle loading from TGA is about 85.9 wt % due to the incomplete polymerization of monomers, which is also observed in PANI-Al_2O_3 PNCs.[47]

Rheological Behavior of the Liquid Epoxy Resin Suspension. Viscosity is an important variable for processing and manufacturing resin and its composites.[53] The study of storage modulus (G') and loss modulus (G'') of the solution is very important for understanding the behaviors of liquid solutions and predicting the nature of NPs and epoxy interactions.[54] The storage modulus measures the stored energy and reflects the elastic portion of the dynamic moduli and the loss modulus is related to the energy dissipation associated with the viscous portion of the dynamic moduli and the motion of the

dx.doi.org/10.1021/am301529t | ACS Appl. Mater. Interfaces 2012, 4, 5613−5624

polymer chains.[55] (The detailed results of G' and G'' are shown in Figure S1 in the Supporting Information.) Briefly, the G' and G'' increase with increasing nanoparticle loadings. The surface functionalization can make Fe_3O_4 NPs uniformly dispersed in the polymer matrix and has more obvious effects on the G' than on G''. The G' increases with increasing temperature for epoxy resin suspensions filled with both u-Fe_3O_4 and f-Fe_3O_4 NPs.

Effect of Nanoparticle Loading. Panels a and b in Figure 2 show the viscosity as a function of shear rate for pure epoxy resin monomers and epon suspensions with different loadings of u-Fe_3O_4 and f-Fe_3O_4 NPs at room temperature. For both u-Fe_3O_4 and f-Fe_3O_4 NPs suspended liquid epon resin, higher viscosity is observed for the higher nanoparticle loadings and lower viscosity are observed for the higher shear rate. The Newtonian behavior is observed in pure epoxy resin as expected with the shear rate lower than 400 1/s and the viscosity decreases at the shear rate higher than 400 1/s, which is due to the entanglement of the epon molecular chains.[56] Compared with pure epoxy resin, the viscosity is decreased in the epoxy resin suspensions filled with 2 wt % NPs, then increases slightly as the NP loading increases to 5 wt % and after that the viscosity increases significantly when the nanoparticle loading further increases to 10 and 20 wt %. In the present work, the decreased viscosity for the epoxy resin suspensions filled with 2 wt % NPs is possibly induced by the sphere-shape NPs. Mackay *et al.*[57] have pointed out that the shape of the NPs is extremely important for the liquid suspensions and only the sphere-shape NPs have shown the decreased viscosity so far. However, when the nanoparticle loading increases, the Fe_3O_4 NPs tend to agglomerate because of the strong interparticle magnetic dipole interactions,[46] form the network structure within the polymer matrix, and increase the resistance of the laminar motion of the fluid.[56] Similar Newtonian behavior is observed at low shear rate (< 400 1/s) for the epoxy resin suspensions filled with a nanoparticle loading of 2 and 5 wt %, and pseudoplastic behavior (viscosity decreases with increasing shear rate, also called shear thinning) is observed within the high shear rate scale (> 400 1/s). The strong shear thinning phenomenon is observed for the epoxy resin suspensions filled with a nanoparticle loading of 10 and 15 wt %, which is due to the fact that the highly loaded NPs increase the solution inertia and make the epon molecular chains easier to be aligned.[58]

Effect of Surface Functionalization. Figure 2c shows the surface functionalization effect on the viscosity of the epoxy resin suspensions with u-Fe_3O_4 and f-Fe_3O_4 NPs at room temperature. The viscosity of the epon resin suspension with f-Fe_3O_4 NPs is a little higher than that of the epon resin suspension with u-Fe_3O_4 NPs, indicating that the surface functionlization increases the interaction of the NPs and epoxy matrix.[59] However, the difference of the viscosity between epoxy resin suspended with u-Fe_3O_4 and f-Fe_3O_4 NPs is diminished at higher shear rate due to the alignment of the Fe_3O_4 NPs in the epoxy resin solutions. This is in consistence with the theoretical expectation (shear thinning) and experimental observation in composites reinforced with fiber fillers.[60]

Effect of Temperature. Temperature is one important factor affecting the viscosity of epoxy resin.[61] The viscosity of epoxy resin suspension with a u-Fe_3O_4 and f-Fe_3O_4 NP loading of 15 wt % is conducted at 25, 70, and 120 °C, Figure 2d. The viscosity of epoxy resin suspensions filled with both u-Fe_3O_4 and f-Fe_3O_4 NPs is observed to be strongly temperature dependent and decreases from 6−7 Pa.s for 25 °C to 0.17 Pa.s for 70 °C, then increases to 1−2 Pa.s for 120 °C at the low shear rate. However, the viscosity difference between epoxy resin suspensions with u-Fe_3O_4 and f-Fe_3O_4 NPs is diminished when the shear rate increases and the viscosity is almost the same (around 0.1 Pa.s) at 70 and 120 °C due to the shear thinning behavior of epon molecular chains.[58] The viscosity of pure epoxy resin decreases with increasing temperature. At high temperature, the obvious phase separation between u-Fe_3O_4 NPs and epoxy monomers is observed during the viscosity measurement, which increases the resistance of the laminar motion of the liquid, thus, the viscosity of epoxy resin suspension with u-Fe_3O_4 NPs is higher than that of epoxy resin suspension with f-Fe_3O_4 NPs, indicating that a better compatibility between f-Fe_3O_4 NPs and epoxy resin.

DMA Properties. Dynamic mechanical analysis (DMA) can characterize the viscoelastic properties of the materials and determine the information of G', G'', and tan δ of cured pure epoxy and its PNCs within the measured temperature range. Figure 3a shows the G′ as a function of temperature of the cured pure epoxy and its PNCs filled with different f-Fe_3O_4 nanoparticle loadings. The G′ values of the cured PNCs filled with a nanoparticle loading of 2, 5, 10, and 15 wt % are observed to be 6.5% (6.23 MPa), 20.7% (7.06 MPa), 183.1% (16.56 MPa), and 95.0% (11.41 MPa) higher than that (5.85 MPa) of the cured pure epoxy within the rubbery state (at 200 °C), respectively (only have the slight change within the glassy state at 30 °C). The G' values of the PNCs filled f-Fe_3O_4 NPs increase with increasing NP loading to 10 wt % and then decrease (15 wt %). The significant increase in G' is ascribed to the stiffness enhancement of the f-Fe_3O_4 NPs in the hosting polymer matrix.[55] The decreased G' (for the PNCs of 15 wt % f-Fe_3O_4 NP loading) is caused by the agglomeration of NPs.[59] G'' as a function of temperature also exhibits the similar trend to G', Figure 3b. The cured epoxy PNCs reinforced with 10 wt % f-Fe_3O_4 NPs exhibit the highest G'' within the measured temperature scale (the same as G'). The maximum peaks of G'', related to the motion of main chains of the epoxy networks at transition from the glassy state to the rubbery state[55] for all the epoxy PNCs, shift to higher temperature (about 5−7 °C) compared with that (76.1 °C) of pure epoxy because of the increased stiffness and constrained friction between polymer chains caused by the added f-Fe_3O_4 NPs.[62]

Figure 3c shows the temperature dependent tanδ of cured pure epoxy and its PNCs. The tanδ is the ratio of G'' to G' and the peak of tan δ is often used to determine the glass transition temperature (T_g) of the materials. As seen in Figure 3c, the T_g of the PNCs shifts to a higher temperature (about 5−7 °C) compared with cured pure epoxy. Unlike 1-d carbon nanotubes and carbon nanofibers, the T_g almost has no change because the less strain is imposed on the polymer chains.[59,62] The height of the tanδ peaks is observed to decrease with increasing f-Fe_3O_4 NPs to 10 wt % and then slightly increase for 15 wt %. This is due to the enhanced stiffness of the PNCs by adding NPs, which is also observed in the layered double hydroxides (LDHs)/epoxy PNCs.[55]

The surface functionalization effect of Fe_3O_4 NPs on the DMA properties of the cured epoxy PNCs is also investigated. Figure 4 shows the G', G'', and tan δ for the cured epoxy PNCs reinforced with both f-Fe_3O_4 NPs at a loading of 5 and 10 wt %, respectively. Both G' and G'' are observed to increase with increasing the nanoparticle loading. G′ is almost identical within the glassy state (at 30 °C) for epoxy PNCs filled with the same u-Fe_3O_4 and f-Fe_3O_4 NP loading, whereas within the rubbery state, G' of the epoxy PNCs reinforced with f-Fe_3O_4 NPs is higher than that of the PNCs reinforced with u-Fe_3O_4 NPs at the same loading,

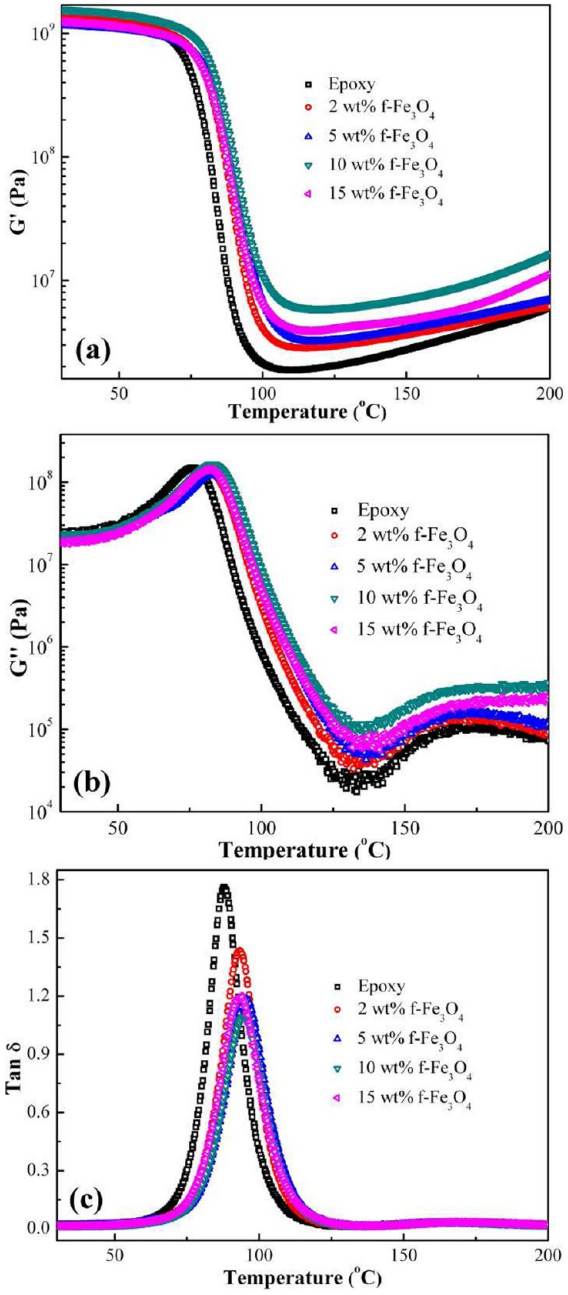

Figure 3. (a) G', (b) G'', and (c) tan δ vs temperature curves for cured pure epoxy and its PNCs with different f-Fe_3O_4 nanoparticle loadings.

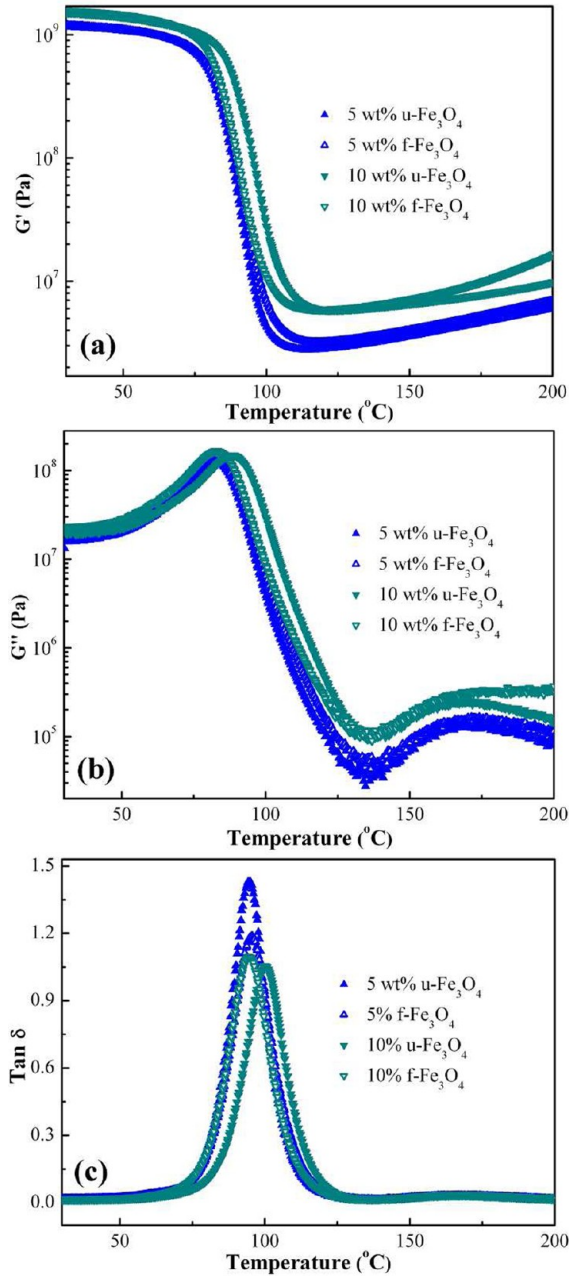

Figure 4. (a) G', (b) G'', and (c) tan δ vs. temperature curves for PNCs filled with 5 and 10 wt % u-Fe_3O_4 and f-Fe_3O_4 nanoparticles, respectively.

Figure 4a. The maximum peaks of G″ for the epoxy PNCs filled with 5 wt % u-Fe_3O_4 and f-Fe_3O_4 NPs are almost the same while it has about 6 °C changes in the epoxy PNCs filled with 10 wt % u-Fe_3O_4 (88.3 °C) and f-Fe_3O_4 (82.9 °C) nanoparticle loading, Figure 4b. The peak of tan δ shifts significantly to higher temperature (about 6 °C) for the cured PNCs filled with the u-Fe_3O_4 NPs and it has only a little shift to a lower temperature (less than 1°C) for the cured PNCs filled with the f-Fe_3O_4 NPs, Figure 4c. It's well-known that T_g reflects the effects of fillers on the segmental motions in polymer composites.[63] In this case, the u-Fe_3O_4 NPs restrict the motions of the polymer chains and T_g increases obviously, however, the f-Fe_3O_4 NPs have less effect on the motion of the polymer chain compared with u-Fe_3O_4 NPs and thus T_g has no obvious change.

Tensile Test. The functionalization effects on the tensile strength (the maximum stress in the stress−strain curve, MPa) and Young's modulus (the slope of the stress−strain curve in the low strain region) are investigated by the tensile test. Figure 5 shows the typical stress−strain curves of the cured pure epoxy, the u-Fe_3O_4 and f-Fe_3O_4 NPs/epoxy PNCs with different nanoparticle loadings. The tensile strength for the cured pure epoxy is about 84.2 MPa, however, for the u-Fe_3O_4 NPs/epoxy PNCs, the tensile strength decreases with increasing nanoparticle loading and is lower than that of cured pure epoxy due to the poor interaction between NPs and epoxy polymer matrix (82.4, 79.3, 60.2 MPa for the PNCs with a nanoparticle loading of 2, 5, and 15 wt %, respectively). Higher tensile strength (97.4 and 93.1 MPa in the f-Fe_3O_4 NPs/epoxy PNCs with a nanoparticle loading of 2 and 5 wt %) is observed compared with that of cured

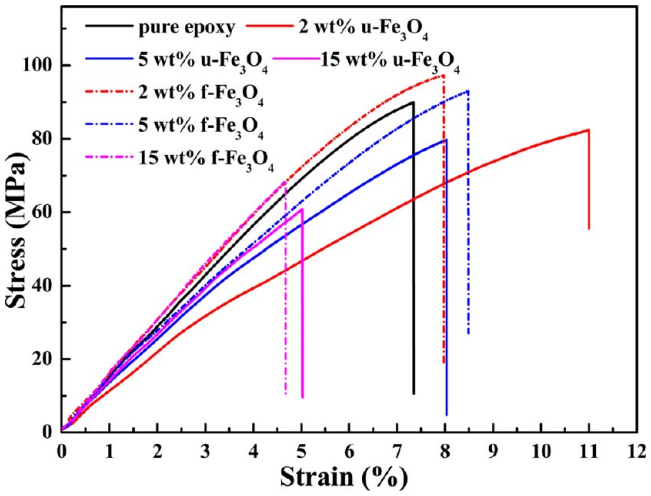

Figure 5. Stress–strain curves of cured epoxy PNCs filled with different loadings of u-Fe_3O_4 and f-Fe_3O_4 NPs.

pure epoxy, respectively, and it decreases to 68.4 MPa when the nanoparticle loading increases further to 15 wt % due to the agglomeration of the NPs, but it's still higher than that of the u-Fe_3O_4 NPs/epoxy PNCs (60.2 MPa). These results indicate that the nanoparticle surface functionalization has significantly improved the tensile strength of epoxy, which is attributed to the enhanced interfacial interaction between NPs and polymer matrix.[30] The Young's modulus of the f-Fe_3O_4/epoxy PNCs is higher than that of the cured pure epoxy and the corresponding epoxy PNCs filled with the u-Fe_3O_4 NPs, indicating that the f-Fe_3O_4 NPs form a stiff interfacial layer between Fe_3O_4 NPs and epoxy to cause a harder polymer deformation.[56] The Young's modulus of the f-Fe_3O_4/epoxy PNCs decreases with increasing f-Fe_3O_4 nanoparticle loadings. The same results are also observed in the MWNTs/epoxy composite systems, arising from the nanoscopic defects of the epoxy matrix by adding more NPs.[64]

Microstructures of Polymer Nanocomposites and Fracture Surface. To investigate the effect of functionalization on the particle distribution, which contributes to the enhanced tensile strength, we show the particle distribution in the cured epoxy PNCs filled with 5 wt % loading of u-Fe_3O_4 and f-Fe_3O_4 NPs after polishing in Figure 6. Figure 6a depicts the surface of cured u-Fe_3O_4/epoxy PNCs. From Figure 6a, the u-Fe_3O_4 NPs are observed agglomerated. The surface of cured f-Fe_3O_4/epoxy PNCs is shown in Figure 6b. The f-Fe_3O_4 NPs are observed uniformly dispersed in the epoxy matrix.

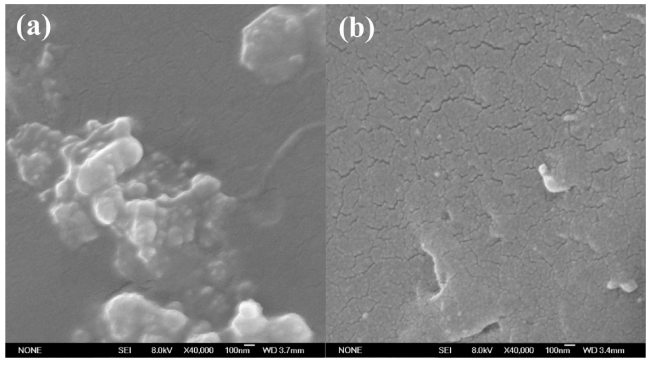

Figure 6. Particle distribution on the cross-sectional surface of cured epoxy PNCs filled with 5 wt % loading of (a) u-Fe_3O_4 and (b) f-Fe_3O_4 NPs after polishing.

Figure 7 shows the SEM microstructures of the fracture surface of the cured pure epoxy and its PNCs filled with 2 and 15 wt % u-Fe_3O_4 and f-Fe_3O_4 NPs. The fracture surface of cured pure epoxy is relatively smooth, Figure 7a, whereas the PNCs exhibit a rough fracture surface, Figure 7b–e. The rough surface is attributed to the matrix shear yielding or polymer deformation between the Fe_3O_4 NPs. Similar results are also observed in the carbon nanofibers reinforced epoxy PNCs.[59] The structural deformation of pure epoxy shows the same direction, Figure 7a, whereas the crack direction of the PNCs is interrupted by the Fe_3O_4 NPs showing random directions (Figure 7b–e). The mechanical properties of the PNCs are strongly related to the interfacial properties of the NPs and epoxy matrix.[65] Interestingly, the fracture surface of f-Fe_3O_4/epoxy PNCs, Figure 7c, e, is very different from that of u-Fe_3O_4/epoxy PNCs, Figure 7b, d. In Figure 7c, for the epoxy PNCs filled with 2 wt % f-Fe_3O_4 NPs, many obviously protruding NPs are observed on the fracture surface and the cracks pass around the NPs without damaging it, which is also found in the alumina NPs reinforced vinyl ester resin PNCs,[15] indicating a good adhesion between the NPs and polymer matrix with an effective load transfer from weak polymer matrix to the strong f-Fe_3O_4 NPs with a resultant higher mechanical strength. The fracture surface of epoxy PNCs with 15 wt % u-Fe_3O_4 and f-Fe_3O_4 NPs is shown in Figure 7d, e. The agglomeration of the NPs is observed on the surface for the 15 wt % u-Fe_3O_4/epoxy PNCs, Figure 7d, which introduces more concentrated stresses on the interface. These observations strongly indicate that the surface functionalization not only improves the particle dispersion but also enhances the particle–epoxy interaction, which causes increased tensile strength.

Magnetic Properties. Magnetization is a phenomenon which defines the response of the induced magnetic dipole moments in a magnetic material to an applied external magnetic field. Figure 8 shows the room temperature magnetic hysteresis loops of u-Fe_3O_4 and f-Fe_3O_4 NPs, epoxy PNCs filled with 15 wt % loading of u-Fe_3O_4 and f-Fe_3O_4 NPs. No hysteresis loops are observed in all the magnetization curves with a zero Oe coercivity, indicating a superparamagnetic behavior.[66] For all the samples, the saturation magnetization (M_s) is not reached even at high magnetic field and determined by the extrapolated saturation magnetization obtained from the intercept of M–H^{-1} at high field.[29,58] The calculated M_s of u-Fe_3O_4 NPs is 57.38 emu/g, which is smaller than that of the bulk Fe_3O_4 (92–100 emu/g).[67] The M_s value of the functionalized Fe_3O_4 NPs after coated with PANI is observed to be saturated at a lower field and is about 48.39 emu/g. The particle loading for the f-Fe_3O_4 NPs estimated from the M_s is found to be 84.33 wt %, which is consistent with the result obtained from TGA, Figure 1h. The M_s value of the epoxy PNCs filled with 15 wt % f-Fe_3O_4 NPs is about 9.49 emu/g. The magnetization of the epoxy PNCs is related to the presence of Fe_3O_4 NPs.[27] The particle loading obtained from the M_s is about 16.4 wt %, which is consistent with the result obtained from TGA (see Figure S2 in the Supporting Information, 15 wt % f-Fe_3O_4). The inset of Figure 8 shows the good magnetic performance of the PNCs, which is attracted by a permanent magnet.

PNCs Formation Mechanism Exploration. PANI, one of the conjugated polymers, consists of alternating amine and imine groups in its polymer backbone.[19] Theoretically, the amine groups can chemically react with the epoxide groups and form a strong chemical bonding. To better elaborate on the reaction

dx.doi.org/10.1021/am301529t | ACS Appl. Mater. Interfaces 2012, 4, 5613–5624

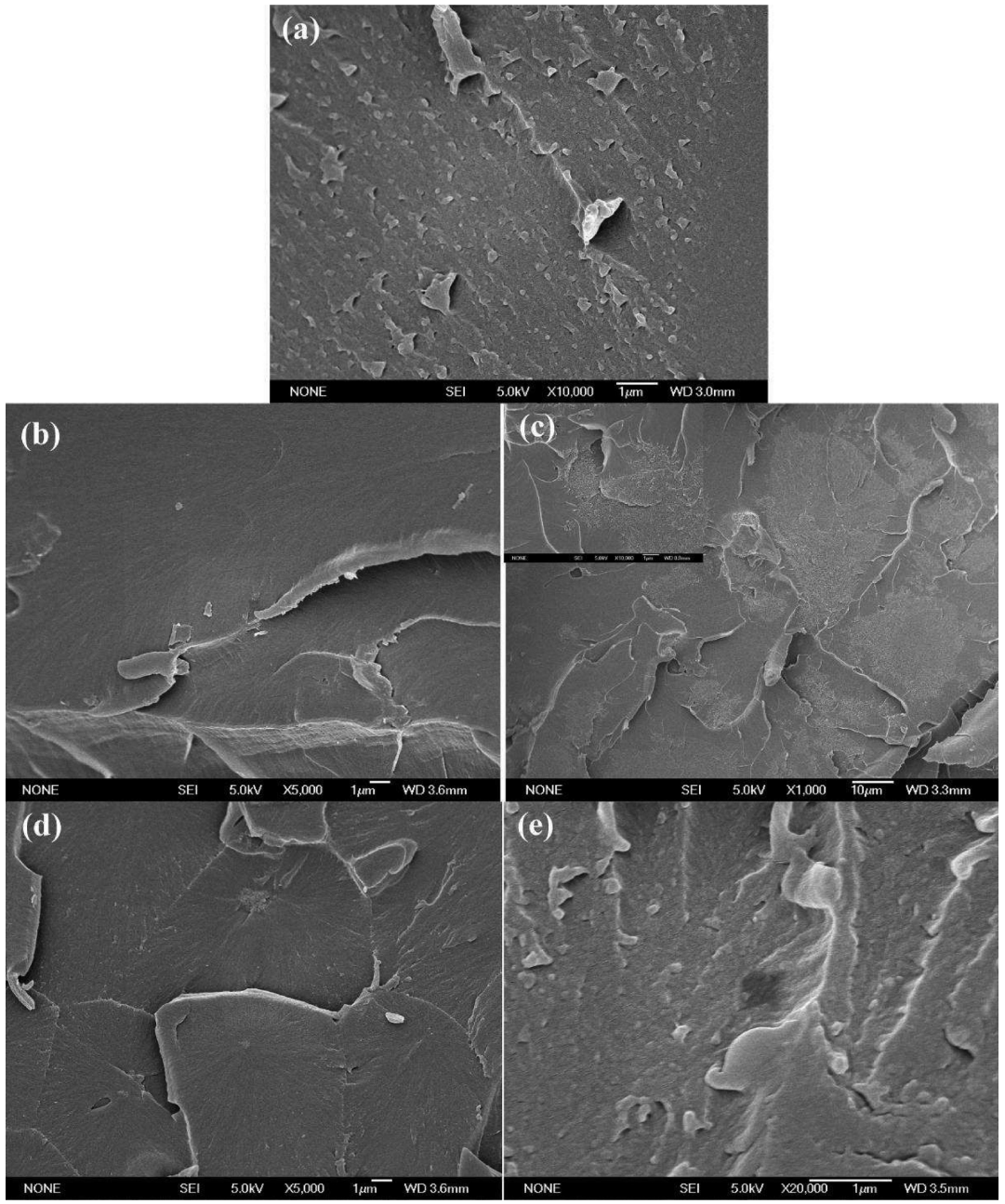

Figure 7. SEM images of fracture surface of (a) cured pure epoxy, and its PNCs filled with (b) 2 wt % u-Fe_3O_4, (c) 2 wt % f-Fe_3O_4, (d) 15 wt % u-Fe_3O_4, and (e) 15 wt % f-Fe_3O_4 NPs.

between PANI on the NP surface and the epoxy resins and to understand the nanocomposite formation mechanism, we have explored the f-Fe_3O_4 NPs and PANI before and after being mixed with epoxy resin monomers with FT-IR, TGA, and DSC.

Figure 9A shows the FT-IR spectra of epoxy monomers/f-Fe_3O_4 NPs before and after curing and washed with acetone. The major differences between the spectrum of f-Fe_3O_4 NPs and that of the f-Fe_3O_4 NPs after epoxy resin curing and washed with acetone samples are observed in the region of 1000 and 1600 cm^{-1}, Figure 9Aa,b. The new peak around 1235 cm^{-1} within the marked pink region in Figure 9Ab appears obviously, which is attributed to the strong absorption of C−O−C stretch vibration[68] and is also observed in the spectrum of the epoxy monomers, Figure 9Ac. These changes indicate that the epoxy monomers have bonded on the f-Fe_3O_4 NPs. The peak around 911 cm^{-1} in the spectrum of the epoxy monomers is attributed to the terminal epoxy group, from which the curing extent can be determined.[69] The FT-IR spectra of the cured pure epoxy, epoxy reinforced with u-Fe_3O_4 and f-Fe_3O_4 NPs are also conducted for further comparison, Figure 9B. After curing process, the peak intensity at around 911 cm^{-1} decreases (but doesn't disappear) in the spectra of cured epoxy and its PNCs filled with u-Fe_3O_4 NPs compared with that of the epoxy monomers, indicating that the curing occurred but was incomplete. However, this peak is almost disappeared in the cured epoxy PNCs filled with f-Fe_3O_4 NPs, indicating that the presence of the PANI coating is beneficial to the curing process and promotes a complete curing. That is, the amine groups from PANI participate in the curing process by reacting with epoxy resin.

dx.doi.org/10.1021/am301529t | *ACS Appl. Mater. Interfaces* 2012, 4, 5613−5624

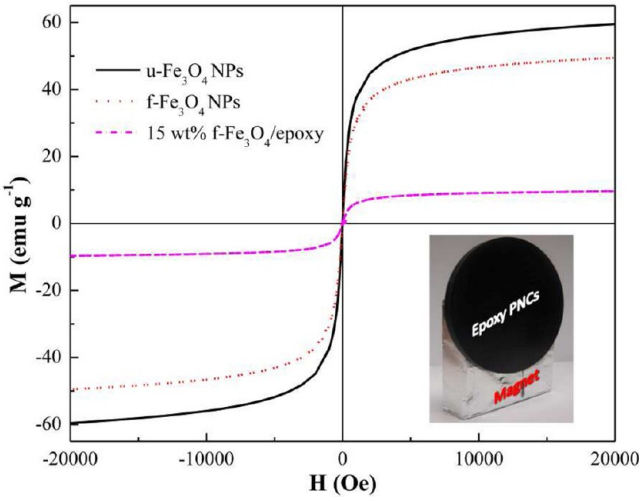

Figure 8. Room-temperature magnetic hysteresis loops of u-Fe_3O_4 and f-Fe_3O_4 NPs and epoxy PNCs filled with 15 wt % f-Fe_3O_4 NPs. Inset shows that PNCs are attracted by a permanent magnet.

Figure 10A shows the thermal decomposition curves of the epoxy resin monomers, PANI/epoxy suspension, f-Fe_3O_4 NPs/epoxy suspension, PANI NPs, and f-Fe_3O_4 NPs after curing and washed with acetone. For the pure epoxy resin monomers, Figure 10Aa, two-stage weight losses are observed within the measured temperature region, which is slightly different from the cured epoxy (refer to the Supporting Iformation, Figure S2, pure epoxy). The first weight oss (200-300 °C) is attributed to the degradation of C−O−C group[70] of epoxy resin monomers. The second decomposition process is from the degradation of benzene ring, similar to the third thermal decomposition process of the cured pure epoxy, see Figure S2 in the Supporting Information. However, for the epoxy resin suspension with PANI NPs, Figure 10Ac, and f-Fe_3O_4 NPs, Figure 10Ab, three weight losses are observed in their decomposition profiles. The extra weight loss from 300 to 500 °C is attributed to the degradation of PANI chains,[51] which is not obvious for the epoxy resin suspension with f-Fe_3O_4 NPs because of the smaller amount of PANI presented compared with the epoxy resin suspension with the same loading of PANI NPs. The TGA curve of the PANI NPs after curing and washed with acetone, Figure 10A, has a slight change compared with that of pure PANI, Figure 1h, in the temperature range of 200−300 °C, which is from the presence of the epon molecules and the degradation of C−O−C group. The decomposition profile of the f-Fe_3O_4 NPs after curing and washed with acetone is similar to that of f-Fe_3O_4 NPs, however, the weight residue is about 75.4%, which is lower than that of f-Fe_3O_4 NPs (85.9%). These results indicate that there are epon molecules attached on PANI after curing and washed with acetone, indicating that there is chemical bonding formed between PANI and epoxide groups.

Figure 10B shows the DSC curves of the epoxy resin monomers, epoxy resin suspension with PANI NPs and f-Fe_3O_4 NPs. For the epoxy monomers (Figure 10Bb), no exothermic peak is observed during the whole procedure. However, the curing exothermic peak (the temperature is around 110 °C) is obviously observed in the epoxy suspension with PANI NPs (Figure 10Bc) and f-Fe_3O_4 NPs (Figure 10Ba), and this peak shifts to a higher temperature for the epoxy suspension with f-Fe_3O_4 NPs due to the presence of Fe_3O_4 NPs, which illustrates that PANI has reacted with the epoxy resin monomers because of the presence of amine groups.

Summarized the aforementioned results, the introduced amine functional groups of PANI in the f-Fe_3O_4 NPs can copolymerize with the epoxy resin to form the PNCs. The proposed PNC formation mechanism is presented in Scheme 1. The functionalized amine groups on the surface of the Fe_3O_4 NPs react with epoxy resin monomers and the Fe_3O_4 NPs can be strongly linked with epoxy matrix through the bridging of the covalent bonding.

CONCLUSION

Magnetic epoxy nanocomposites reinforced with different u-Fe_3O_4 and f-Fe_3O_4 nanoparticle loadings have been prepared. The rheological measurements of the epoxy nanocomposite suspensions filled with different loadings of u-Fe_3O_4 and f-Fe_3O_4 NPs are performed at different shear rates and frequencies. The viscosity increases with increasing NP loadings and decreases with increasing shear rates. The G' and G'' increase with increasing NP loadings. The surface functionalization can make Fe_3O_4 NPs uniformly dispersed in the polymer matrix and has more obvious effects on the G' than on G''. The DMA results show that the polymer chains have become stiffer after adding the functionalized Fe_3O_4 NPs and the T_g has shifted to a higher temperature (about 5−7 °C) compared with that of cured pure epoxy. The resulting enhanced mechanical properties are attributed to the strong interfacial interaction between f-Fe_3O_4 NPs and epoxy polymer matrix and uniform NP distribution after

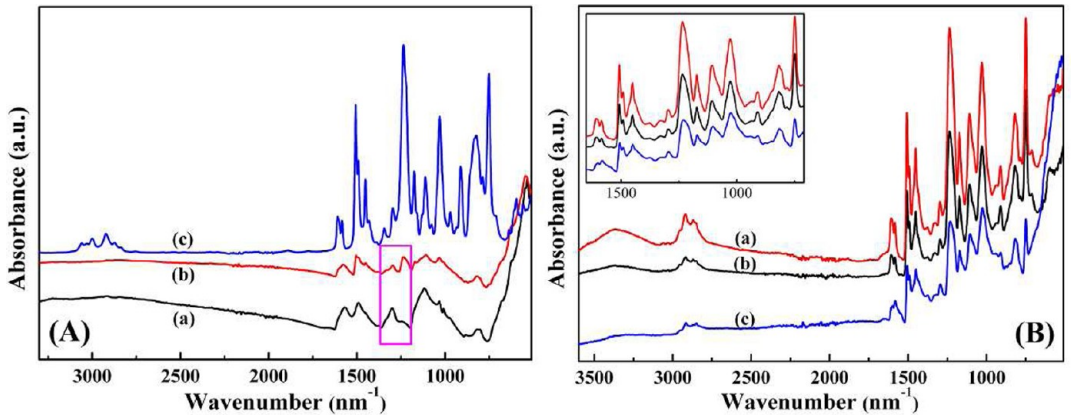

Figure 9. FT-IR spectra of the (A) (a) f-Fe_3O_4 NPs, (b) f-Fe_3O_4 NPs after washed with acetone, and (c) epoxy monomers; (B) (a) cured epoxy with 15 wt % loading u-Fe_3O_4 NPs, (b) cured epoxy, and (c) cured epoxy with 15 wt % loading f-Fe_3O_4 NPs.

dx.doi.org/10.1021/am301529t | ACS Appl. Mater. Interfaces 2012, 4, 5613−5624

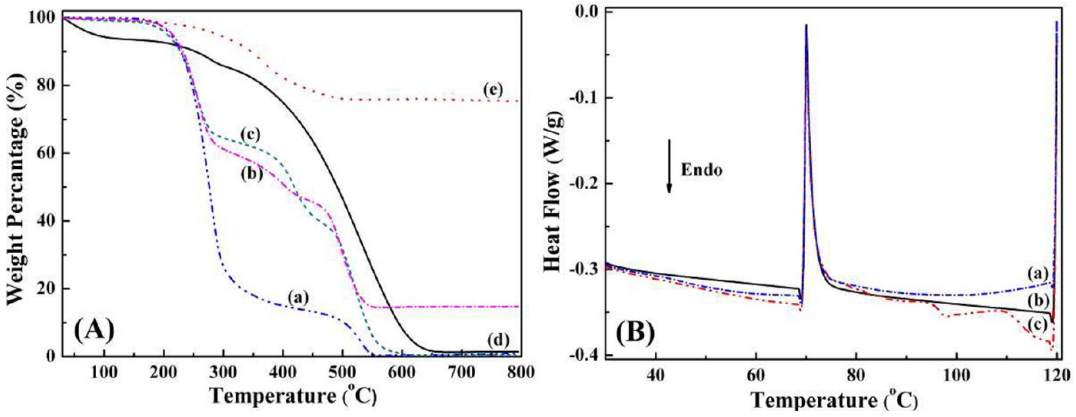

Figure 10. (A) TGA curves of (a) epoxy monomer, (b) epon suspension with f-Fe_3O_4 NPs, (c) epon suspension with PANI NPs, (d) PANI NPs, and (e) f-Fe_3O_4 NPs after wash with acetone; (B) DSC curves of (a) epon suspension with f-Fe_3O_4 NPs, (b) epon monomers, (c) epon suspension with PANI NPs.

Scheme 1. Proposed Polymer Nanocomposite Formation Mechanism

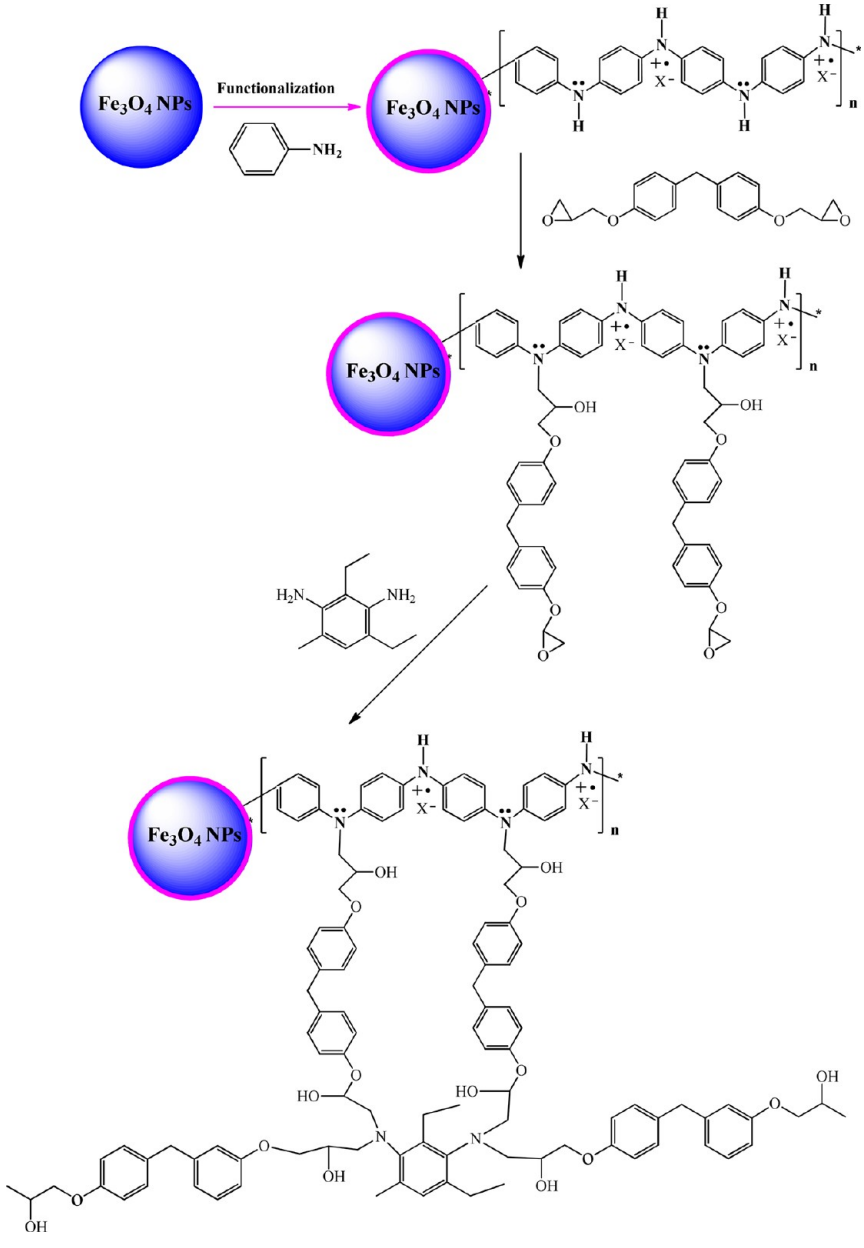

dx.doi.org/10.1021/am301529t | ACS Appl. Mater. Interfaces 2012, 4, 5613−5624

surface functionalization by the PANI layer. The rough fracture surface of the PNCs filled with f-Fe_3O_4 NPs clearly interprets the effective load transfer from the weaker epoxy matrix to the stronger the f-Fe_3O_4 NPs and good interfacial interaction between the f-Fe_3O_4 NPs and the hosting epoxy matrix. The enhanced thermal stability is observed in the f-Fe_3O_4 NP filled epoxy PNCs compared with that of cured pure epoxy and its PNCs filled with u-Fe_3O_4 NPs. These magnetic epoxy PNCs show good magnetic properties and can be attached by a permanent magnet. The PNCs formation mechanism is proposed based on the f-Fe_3O_4 NPs and PANI before and after being mixed with epoxy matrix as analyses by the FT-IR, TGA, and DSC, which is responsible for the observed enhanced mechanical properties.

■ ASSOCIATED CONTENT

Supporting Information

The effects of nanoparticle loading, surface functionality and temperature on the storage modulus (G'') and loss modulus (G'') of epoxy resin suspensions; TGA analysis are in the supporting materials. This material is available free of charge via the Internet at http://pubs.acs.org.

■ AUTHOR INFORMATION

Corresponding Author

*E-mail: suying.wei@lamar.edu (S.W.); huangyd@hit.edu.cn (Y.H.); zhanhu.guo@lamar.edu (Z.G.).

Present Address

[∇]Department of Chemistry and Physics, Fayetteville State University, Fayetteville, North Carolina 28301, United States.

Notes

The authors declare no competing financial interest.

■ ACKNOWLEDGMENTS

This project is financially supported by the National Science Foundation Nanoscale Interdisciplinary Research Team, and Materials Processing and Manufacturing (CMMI 10-30755). The authors appreciate Miss Xi Zhang for the operations of rheological property, differential scanning calorimeter (DSC), thermogravimetric analysis (TGA), and dynamic mechanical analysis (DMA). D.Y. acknowledges support from the NSF under Grant No. DMR 10-05764. H.G. acknowledges the support from China Scholarship Council.

■ REFERENCES

(1) Akatsuka, M.; Takezawa, Y.; Amagi, S. *Polymer* **2001**, *42*, 3003−3007.
(2) Jyotishkumar, P.; Koetz, J.; Tiersch, B.; Strehmel, V.; Özdilek, C.; Moldenaers, P.; Hässler, R.; Thomas, S. *J. Phys. Chem. B* **2009**, *113*, 5418−5430.
(3) Hsiao, K.-T.; Alms, J.; Advani, S. G. *Nanotechnology* **2003**, *14*, 791−793.
(4) Tunce, E.; Sauers, I.; James, D. R.; Ellis, A. R.; Paranthaman, M. P.; Aytuğ, T.; Sathyamurthy, S.; More, K. L.; Li, J.; Goyal, A. *Nanotechnology* **2007**, *18*, 025703.
(5) Toldy, A.; Szolnoki, B.; Marosi, G. *Polym. Degrad. Stab.* **2011**, *96*, 371−376.
(6) Liu, Y.; Wei, H.; Wu, S.; Guo, Z. *Chem. Eng. Technol.* **2012**, *35*, 713−719.
(7) Gonzalez-Campo, A.; Orchard, K. L.; Sato, N.; Shaffer, M. S. P.; Williams, C. K. *Chem. Commun.* **2009**, 4034−4036.
(8) Olad, A.; Barati, M.; Behboudi, S. *Prog. Org. Coat.* **2012**, *74*, 221−227.
(9) Bao, C.; Guo, Y.; Song, L.; Kan, Y.; Qian, X.; Hu, Y. *J. Mater. Chem.* **2011**, *21*, 13290−13298.
(10) Zhang, C.; Wei, H.; Liu, Y.; Tan, H.; Guo, Z. *High Perform. Polym.* **2012**, DOI: 10.1177/0954008312449846.
(11) Wang, D.; Kou, R.; Choi, D.; Yang, Z.; Nie, Z.; Li, J.; Saraf, L. V.; Hu, D.; Zhang, J.; Graff, G. L.; Liu, J.; Pope, M. A.; Aksay, I. A. *ACS Nano* **2010**, *4*, 1587−1595.
(12) Chan, C.-M.; Wu, J.; Li, J.-X.; Cheung, Y.-K. *Polymer* **2002**, *43*, 2981−2992.
(13) Guo, Z.; Wei, S.; Shedd, B.; Scaffaro, R.; Pereira, T.; Hahn, H. T. *J. Mater. Chem.* **2007**, *17*, 806−813.
(14) Wang, Z.; Yang, X.; Wang, Q.; Hahn, H. T.; Lee, S.-g.; Lee, K.-H.; Guo, Z. *Int. J. Smart Nano. Mater.* **2011**, *2*, 176−193.
(15) Guo, Z.; Pereira, T.; Choi, O.; Wang, Y.; Hahn, H. T. *J. Mater. Chem.* **2006**, *16*, 2800−2808.
(16) Dyke, C. A.; Tour, J. M. *Nano Lett.* **2003**, *3*, 1215−1218.
(17) Kang, Y.; Taton, T. A. *J. Am. Chem. Soc.* **2003**, *125*, 5650−5651.
(18) Tang, L.-c.; Zhang, H.; Han, J.-h.; Wu, X.-p.; Zhang, Z. *Compos. Sci. Technol.* **2011**, *72*, 7−13.
(19) Pron, A.; Rannou, P. *Prog. Polym. Sci.* **2002**, *27*, 135−190.
(20) Lima, E., Jr.; Brandl, A. J.; Arelaro, A. D.; Goya, G. F. *J. Appl. Phys.* **2006**, *99*, 083908.
(21) Liu, F.; Cao, P. J.; Zhang, H. R.; Tian, J. F.; Xiao, C. W.; Shen, C. M.; Li, J. Q.; Gao, H. J. *Adv. Mater.* **2005**, *17*, 1893−1897.
(22) Ding, N.; Yan, N.; Ren, C.; Chen, X. *Anal. Chem.* **2010**, *82*, 5897−5899.
(23) Maeng, J. H.; Lee, D.-H.; Jung, K. H.; Bae, Y.-H.; Park, I.-S.; Jeong, S.; Jeon, Y.-S.; Shim, C.-K.; Kim, W.; Kim, J.; Lee, J.; Lee, Y.-M.; Kim, J.-H.; Kim, W.-H.; Hong, S.-S. *Biomaterials* **2010**, *31*, 4995−5006.
(24) Santos, F. J.; Varanda, L. C.; Ferracin, L. C.; Jafelicci, M. *J. Phys. Chem. C* **2008**, *112*, 5301−5306.
(25) Gupta, V. K.; Agarwal, S.; Saleh, T. A. *Water Res.* **2011**, *45*, 2207−2212.
(26) Guo, Z.; Park, S.; Hahn, H. T.; Wei, S.; Moldovan, M.; Karki, A. B.; Young, D. P. *J. Appl. Phys.* **2007**, *101*, 09M511.
(27) Guo, Z.; Lee, S. E.; Kim, H.; Park, S.; Hahn, H. T.; Karki, A. B.; Young, D. P. *Acta Mater.* **2009**, *57*, 267−277.
(28) Zhu, J.; Wei, S.; Haldolaarachchige, N.; Young, D. P.; Guo, Z. *J. Phys. Chem. C* **2011**, *115*, 15304−15310.
(29) Guo, Z.; Henry, L. L.; Palshin, V.; Podlaha, E. J. *J. Mater. Chem.* **2006**, *16*, 1772−1777.
(30) Guo, Z.; Lei, K.; Li, Y.; Ng, H. W.; Hahn, H. T. *Compos. Sci. Technol.* **2008**, *68*, 1513−1520.
(31) Wei, S.; Wang, Q.; Zhu, J.; Sun, L.; Lin, H.; Guo, Z. *Nanoscale* **2011**, *3*, 4474−4502.
(32) Yi, D. K.; Lee, S. S.; Ying, J. Y. *Chem. Mater.* **2006**, *18*, 2459−2461.
(33) Gass, J.; Poddar, P.; Almand, J.; Srinath, S.; Srikanth, H. *Adv. Funct. Mater.* **2006**, *16*, 71−75.
(34) Zhu, J.; Gu, H.; Rapole, S. B.; Luo, Z.; Pallavkar, S.; Haldolaarachchige, N.; Benson, T. J.; Ho, T. C.; Hopper, J.; Young, D. P.; Wei, S.; Guo, Z. *RSC Adv.* **2012**, *2*, 4844−4856.
(35) Zhu, J.; Wei, S.; Gu, H.; Rapole, S. B.; Wang, Q.; Luo, Z.; Haldolaarachchige, N.; Young, D. P.; Guo, Z. *Environ. Sci. Technol.* **2012**, *46*, 977−985.
(36) Chen, X.; Li, L.; Sun, X.; Liu, Y.; Luo, B.; Wang, C.; Bao, Y.; Xu, H.; Peng, H. *Angew. Chem. Int. Ed.* **2011**, *50*, 5486−5489.
(37) Schmidt, A. M. *Macromol. Rapid Commun.* **2006**, *27*, 1168−1172.
(38) Guo, Z.; Shin, K.; Karki, A.; Young, D.; Kaner, R.; Hahn, H. *J. Nanopart. Res.* **2009**, *11*, 1441−1452.
(39) Krishnamoorti, R.; Giannelis, E. P. *Macromolecules* **1997**, *30*, 4097−4102.
(40) Solomon, M. J.; Almusallam, A. S.; Seefeldt, K. F.; Somwangthanaroj, A.; Varadan, P. *Macromolecules* **2001**, *34*, 1864−1872.
(41) Potts, J. R.; Dreyer, D. R.; Bielawski, C. W.; Ruoff, R. S. *Polymer* **2011**, *52*, 5−25.
(42) Du, F.; Scogna, R. C.; Zhou, W.; Brand, S.; Fischer, J. E.; Winey, K. I. *Macromolecules* **2004**, *37*, 9048−9055.
(43) Liu, C.; Zhang, J.; He, J.; Hu, G. *Polymer* **2003**, *44*, 7529−7532.

(44) Kim, H.; Macosko, C. W. *Macromolecules* **2008**, *41*, 3317−3327.
(45) Zhu, J.; Wei, S.; Yadav, A.; Guo, Z. *Polymer* **2010**, *51*, 2643−2651.
(46) Gu, H.; Huang, Y.; Zhang, X.; Wang, Q.; Zhu, J.; Shao, L.; Haldolaarachchige, N.; Young, D. P.; Wei, S.; Guo, Z. *Polymer* **2012**, *53*, 801−809.
(47) Zhu, J.; Wei, S.; Zhang, L.; Mao, Y.; Ryu, J.; Haldolaarachige, N.; Young, D. P.; Guo, Z. *J. Mater. Chem.* **2011**, *21*, 3952−3959.
(48) Zhu, J.; Wei, S.; Zhang, L.; Mao, Y.; Ryu, J.; Karki, A. B.; Young, D. P.; Guo, Z. *J. Mater. Chem.* **2011**, *21*, 342−348.
(49) Mahmoudi, M.; Simchi, A.; Imani, M.; Milani, A. S.; Stroeve, P. *J. Phys. Chem. B* **2008**, *112*, 14470−14481.
(50) Mavinakuli, P.; Wei, S.; Wang, Q.; Karki, A. B.; Dhage, S.; Wang, Z.; Young, D. P.; Guo, Z. *J. Phys. Chem. C* **2010**, *114*, 3874−3882.
(51) Xuan, S.; Wang, Y. X. J.; Leung, K. C. F.; Shu, K. *J. Phys. Chem. C* **2008**, *112*, 18804−18809.
(52) Feng, X.; Mao, C.; Yang, G.; Hou, W.; Zhu, J. *Langmuir* **2006**, *22*, 4384−4389.
(53) Sui, G.; Zhang, Z.-G.; Chen, C.-Q.; Zhong, W.-H. *Mater. Chem. Phys.* **2003**, *78*, 349−357.
(54) Yoo, B. *J. Food Eng.* **2004**, *65*, 459−463.
(55) Hsueh, H.-B.; Chen, C.-Y. *Polymer* **2003**, *44*, 5275−5283.
(56) Zhu, J.; Wei, S.; Ryu, J.; Sun, L.; Luo, Z.; Guo, Z. *ACS Appl. Mater. Interfaces* **2010**, *2*, 2100−2107.
(57) Tuteja, A.; Duxbury, P. M.; Mackay, M. E. *Macromolecules* **2007**, *40*, 9427−9434.
(58) Zhang, D.; Karki, A. B.; Rutman, D.; Young, D. P.; Wang, A.; Cocke, D.; Ho, T. H.; Guo, Z. *Polymer* **2009**, *50*, 4189−4198.
(59) Zhu, J.; Wei, S.; Ryu, J.; Budhathoki, M.; Liang, G.; Guo, Z. *J. Mater. Chem.* **2010**, *20*, 4937−4948.
(60) Pötschke, P.; Fornes, T. D.; Paul, D. R. *Polymer* **2002**, *43*, 3247−3255.
(61) Pahl, M. H.; Hesekamp, D. *Rheology* **1993**, *3*, 97−104.
(62) Liu, T.; Phang, I. Y.; Shen, L.; Chow, S. Y.; Zhang, W.-D. *Macromolecules* **2004**, *37*, 7214−7222.
(63) Brostow, W.; Chiu, R.; Kalogeras, I. M.; Vassilikou-Dova, A. *Mater. Lett.* **2008**, *62*, 3152−3155.
(64) Ogasawara, T.; Moon, S.-Y.; Inoue, Y.; Shimamura, Y. *Compos. Sci. Technol.* **2011**, *71*, 1826−1833.
(65) Eitan, A.; Jiang, K.; Dukes, D.; Andrews, R.; Schadler, L. S. *Chem. Mater.* **2003**, *15*, 3198−3201.
(66) Xuan, S.; Hao, L.; Jiang, W.; Gong, X.; Hu, Y.; Chen, Z. *J. Magn. Magn. Mater.* **2007**, *308*, 210−213.
(67) Hu, P.; Zhang, S.; Wang, H.; Pan, D.; Tian, J.; Tang, Z.; Volinsky, A. A. *J. Alloys Compd.* **2011**, *509*, 2316−2319.
(68) Parikh, S. J.; Chorover, J. *Langmuir* **2006**, *22*, 8492−8500.
(69) Nikolic, G.; Zlatkovic, S.; Cakic, M.; Cakic, S.; Lacnjevac, C.; Rajic, Z. *Sensors* **2010**, *10*, 684−696.
(70) Santander, C. M. G.; Rueda, S. M. G.; Silva, N. de L. da; Camargo, C. L. de; Kieckbusch, T. G.; Maciel, M. R. W. *Fuel* **2012**, *92*, 158−161.